Supplementary Materials

Due to the limitation of the length of our manuscript, some critical issues, from our perspective, related to the major findings of our work cannot be explained in detail in the manuscript. Therefore, we have prepared the following supplementary materials to elaborate the critical issues as following:

1. **Why is the negative Moist Potential Vorticity (MPV) considered as a cause, not a result (byproduct) of the convection in this case?**

   In many previous studies on the diagnosis of heavy precipitation events in the mesoscale meteorology, a negative Moist Potential Vorticity (MPV) is often indicative of atmospheric instability (e.g., Zhang and Cho,1992; Wu et al., 1995; Ullah and Gao, 2013; Gao et al., 2002; Yao et al. 2020; liu et al.,2022). As shown in Figure 1 below, at 0300 UTC, a relatively strong negative MPV region can be found within the cold pool (CP) over the southern area of the Kunlun Mountains (represented by the dashed purple ellipse in the Figure 1a below). At 0330 UTC (Figure 1b), a relatively weak cloud (indicated by the black contour in the dashed purple ellipse) was developed near the intense negative MPV area. Simultaneously, the strong negative MPV region diminishes, indicating the release of unstable energy to some extent.

   Hence, it can be inferred that negative MPV was not a result or byproduct of the rainfall cloud. Subsequently, as the CP moved towards the northern slope of the Kunlun Mountains, a relatively strong negative MPV region still exists at the leading edge of the CP the CP (Figure 1c). By 0430 UTC (Figure 1d), the previously strong negative MPV weakens to some extent, while the rainfall cloud further development. The release of unstable energy corresponds roughly with the significant developmental trend of rainfall cloud. Therefore, it can be inferred that the instability reflected by negative MPV provided crucial conditions for the convection initiation (CI) of rainfall cloud.

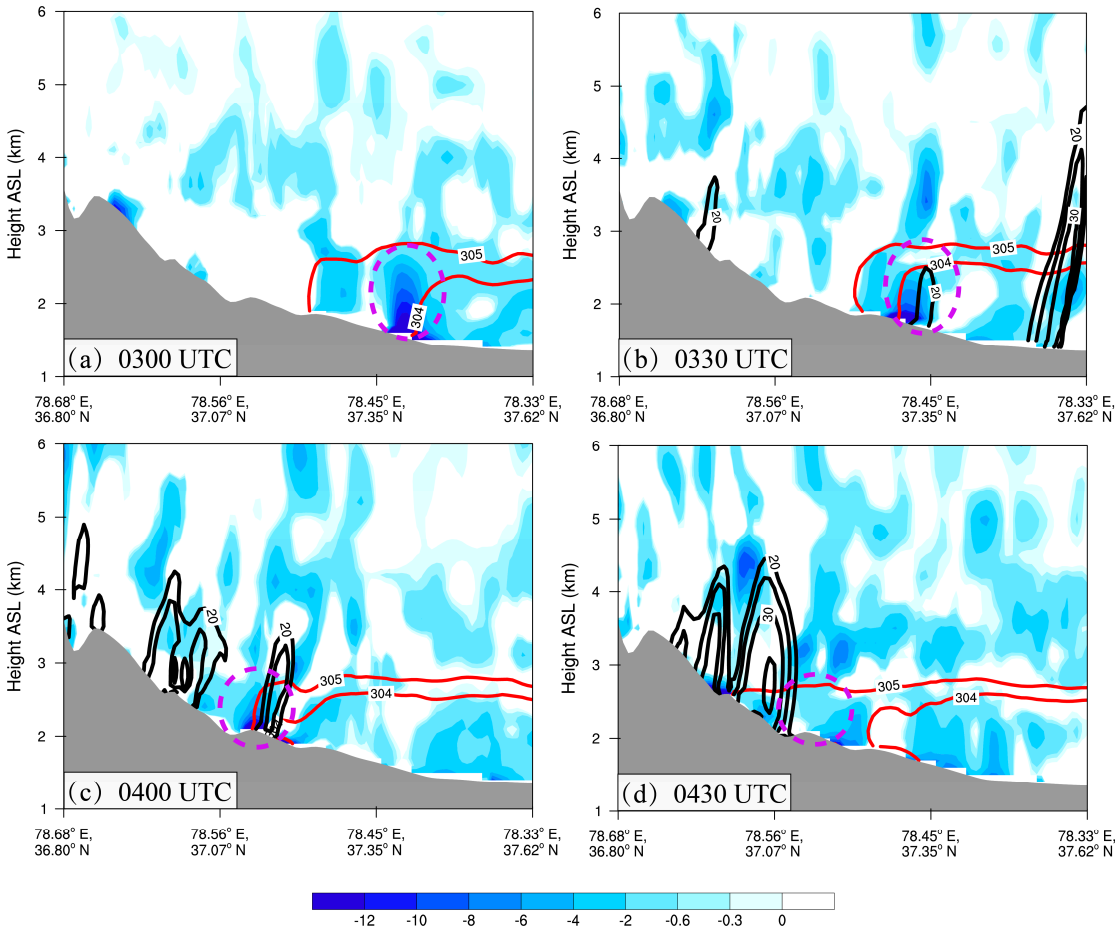

Figure S1. (a-d) Vertical cross section of the moist potential vorticity (MPV, shading, units: PVU, 1 PVU=10^{-6} m^2 K s^{-1} kg^{-1}) and composed reflectivity (black solid contours, units: dBZ) along the line AB at 0300, 0330, 0400 and 0430 UTC on 15 June 2021, respectively. The red solid lines (304 K and 305 K potential temperature contours) indicate the thermal boundary of the cold pool, the gray shading indicates the topography, and the specific time is shown in the lower left corner of each panel.

Moreover, it can be observed from Figure 2 that during the period of vigorous development of short-duration heavy rainfall cloud, the near-surface negative Moist Potential Vorticity (MPV) gradually weakens over the northern slope of the Kunlun Mountains. From 0600 UTC (Figure 2a) to 0630 UTC (Figure 2b), as the near-surface negative MPV intensity significantly decreases (indicated by the purple dashed ellipse), the rainfall cloud experience develop rapidly. From 0700 UTC (Figure 2c) to 0730 UTC (Figure 2d), the rainfall cloud continue to develop vigorously, while the negative MPV intensity near the surface and below approximately 2 km AGL (Above Ground Level) diminishes notably (indicated by the purple dashed ellipse). Consequently, it can be inferred once again that negative MPV is not a result or byproduct of the rainfall cloud.

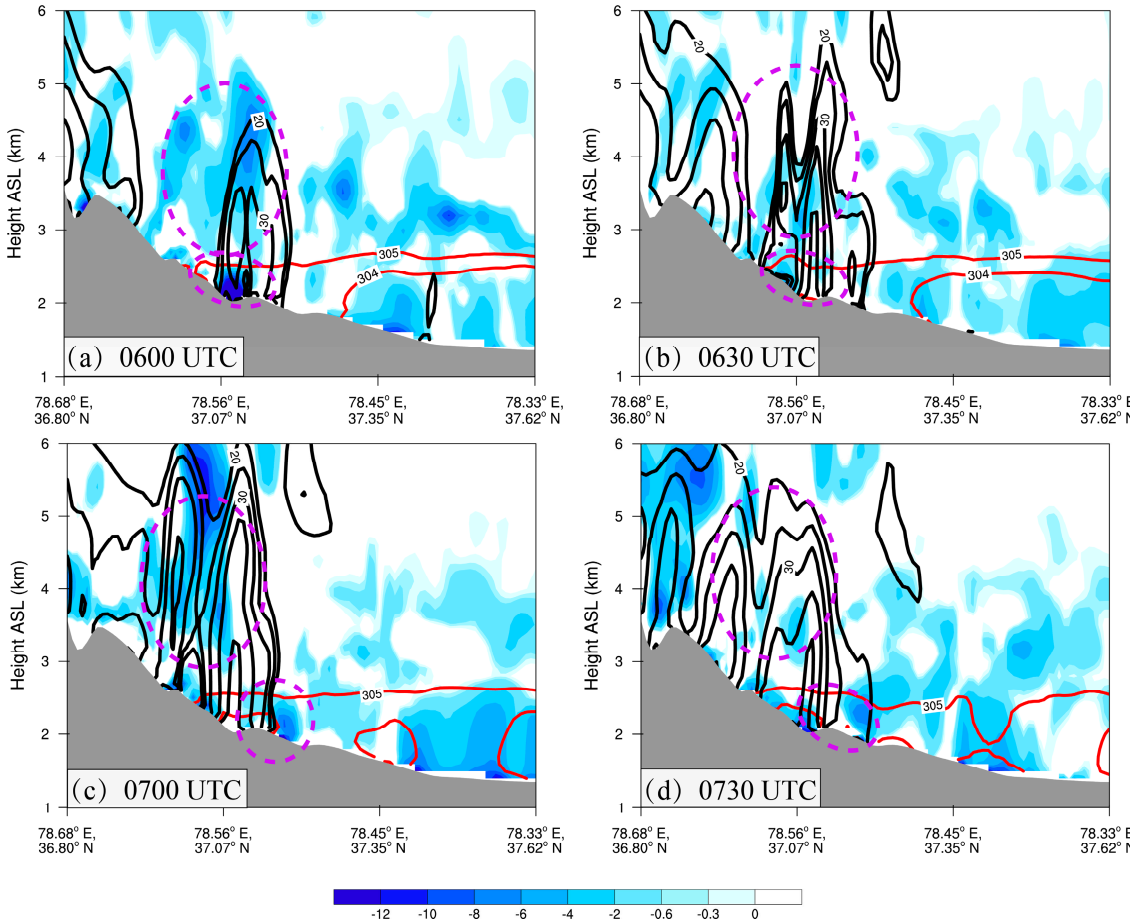

Figure S2. (a-d) Vertical cross section of the moist potential vorticity (MPV, shading, units: PVU, 1 PVU=10^{-6} m^2 K s^{-1} kg^{-1}) and composed reflectivity (black solid contours, units: dBZ) along the line AB at 0600, 0630, 0700 and 0730 UTC on 15 June 2021, respectively. The red solid lines (304 K and 305 K potential temperature contours) indicate the thermal boundary of the cold pool, the gray shading indicates the topography, and the specific time is shown in the lower left corner of each panel.

Since the MPV had obvious advantages in diagnosing the rainfall (i.e., it can be considered as a useful and effective quantity for related diagnostic analysis), it can be deduced that the negative MPV can be or should be considered as an indicator of the weather system's cause, rather than a result or byproduct of the weather system. Therefore, the MPV can also be used in our present study as a "diagnostic tool" in order to understand the cause of the CI of the rainstorm to some extent.

2. Why is frontogenesis responsible for the excitation of unstable energy, not a result (byproduct) in this rainstorm?

The frontal genesis at the leading edge of the CP was considered to be a lifting mechanism that releases unstable energy, thus believed to play a crucial role in the development of this heavy rainfall event. Many studies have also mentioned similar conclusions in their investigations. For example, Schultz and Schumacher (2010) stated that the release of conditional symmetric instability (CSI) was predicated upon slantwise air parcel lifting beyond the lifting condensation level to the level of free slantwise convection (LFSC). They also claimed that the frontogenetical circulation is one of the mechanisms that can produce an ascent flow required to lift an air parcel forcibly to its LFSC. Furthermore, Liu et al. (2022), an extreme heavy rainfall event in the eastern Tianshan region of China was investigated, and it was found that the intense rainfall resulted from the lifting of unstable layering induced by frontal genesis.

Figures 3 and 4 depict the relationship between the CI of rainfall cloud and frontal genesis during the same time periods as Figures 1 and 2. As shown in Figures 3a and 3b at 0300 UTC and 0330 UTC, a relatively strong frontal genesis function was observed within the CP over the southern area of the Kunlun Mountains (indicated by the purple dashed ellipse). However, there was no significant development of rainfall cloud at this time. At 0400 UTC (Figure 3c), the frontal genesis function at the near-surface level (indicated by the purple dashed ellipse) diminishes to some extent, and distinct rainfall cloud start to form by 0430 UTC (Figure 3d). Therefore, it can be inferred that frontal genesis was not a result of the rainfall cloud. Furthermore, at 0600 UTC (Figure 4a) and 0700 UTC (Figure 4b), the frontal genesis function at the near-surface level over the northern slope of the Kunlun Mountains weakens to some extent by 0630 UTC (Figure 4c) and 0730 UTC (Figure 4d), respectively, and the rainfall cloud continue to further develop. It can be concluded once again that frontal genesis was not a result or byproduct of the rainfall cloud.

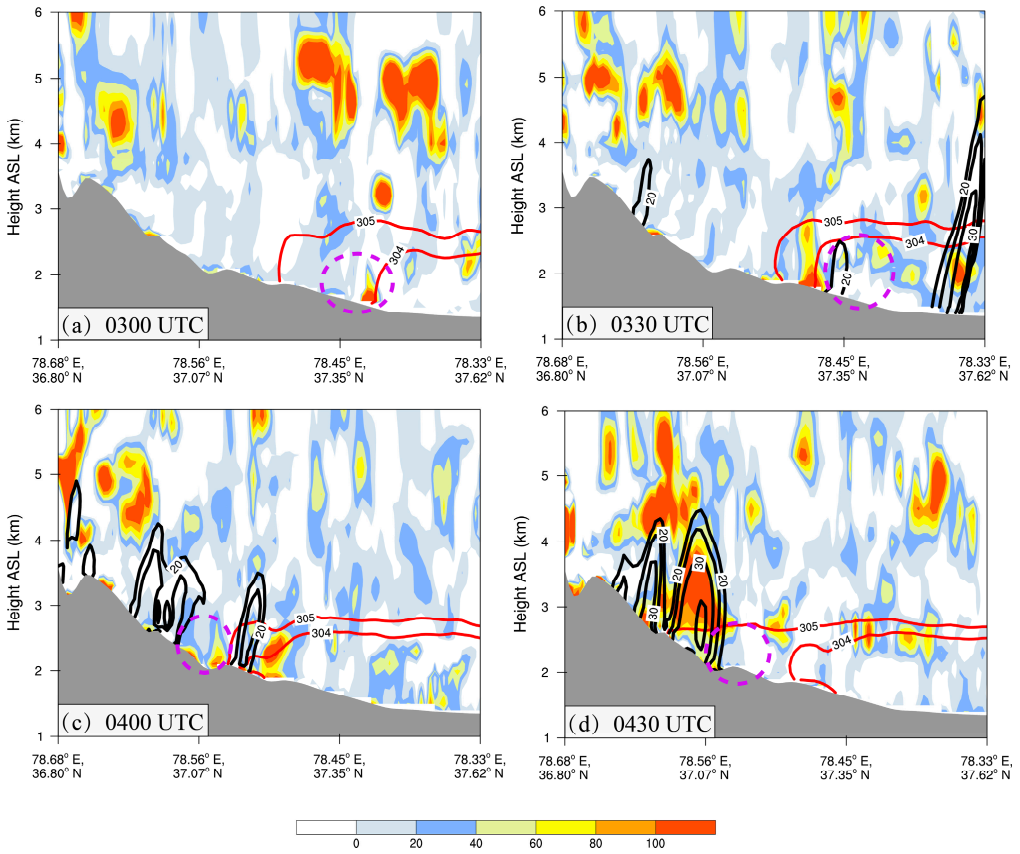

Figure S3. (a-d) Vertical cross-section of the total frontogenesis (Ft) (shading, units: 10^{-8} K m^{-1} s^{-1}) and composed reflectivity (black solid contours, units: dBZ) along the line AB (shown in Figure 8) at 0300, 0330, 0400 and 0430 UTC on 15 June 2021, respectively. The red solid lines (304 K and 305 K potential temperature contours) indicate the thermal boundary of the cold pool, the gray shading indicates the topography, and the specific time is shown in the lower left corner of each panel.

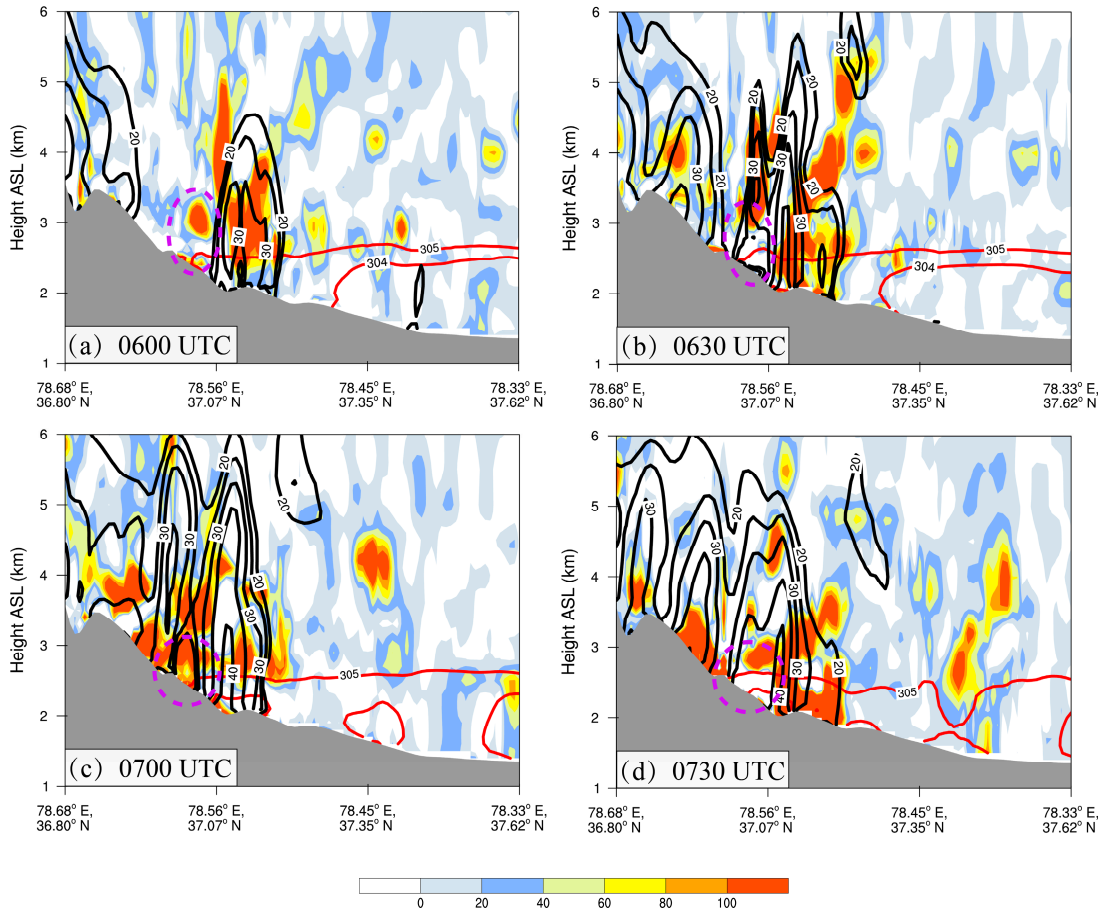

Figure S4. (a-d) Vertical cross-section of the total frontogenesis (Ft) (shading, units: 10^{-8} K m^{-1} s^{-1}) and composed reflectivity (black solid contours, units: dBZ) along the line AB (shown in Figure 8) at 0600, 0630, 0700 and 0730 UTC on 15 June 2021, respectively. The red solid lines (304 K and 305 K potential temperature contours) indicate the thermal boundary of the cold pool, the gray shading indicates the topography, and the specific time is shown in the lower left corner of each panel.

3. Why is there a large wind speed at 2500m ASL on the north slope of Kunlun Mountain before the Convection Initiation?

From the horizontal wind field perspective, a mesoscale vortex existed over our research area. Prior to convective initiation, a boundary layer jet (BLJ) has formed over the northern slope of the Kunlun Mountains. Even before the arrival of the CP (Figures 5a-c), the BLJ exhibits convergence over the northern slope of the Kunlun Mountains. After the CP arrived (Figure 5d), convection was triggered in conjunction with the convergence at the leading edge of the cold pool. Following convective initiation, during 0530 UTC (Figure 5e) to 0630 UTC (Figure 5f), the area of maximum horizontal wind speed over the northern slope of the Kunlun Mountains shifts southeastward.

According to the findings of Du et al. (2014), the formation of BLJ was closely related to factors such as valley wind circulation. To analyze the reasons for the formation of BLJs, we plotted the horizontal pressure field and vertical velocity corresponding to the relevant time periods (Figures 6a-f). From 0130 UTC to 0430 UTC, a low-pressure center moving southeastward was present over the northern slope of the Kunlun Mountains, and the region with a

large horizontal pressure gradient corresponds to the area of strong BLJ, indicating that the formation and changes in the region of strong BLJ are related to the movement of the low-pressure center. During 0530 UTC to 0630 UTC, the horizontal pressure gradient increases, and the corresponding BLJ wind speed also increases. Figure 7 shows the distribution of vertical velocity at 2500m above sea level (ASL). From 0130 UTC to 0630 UTC (Figures 7a-f), prevailing upslope winds are observed over the northern slope of the Kunlun Mountains, resulting in a significant increase in vertical velocity in the research area.

Therefore, we can infer that the formation of BLJ at approximately 2500m ASL over the northern slope of the Kunlun Mountains was influenced by both the movement of the low-pressure center and the enhancement of valley winds. These BLJ, in conjunction with the leading edge of the cold pool, trigger the convective system.

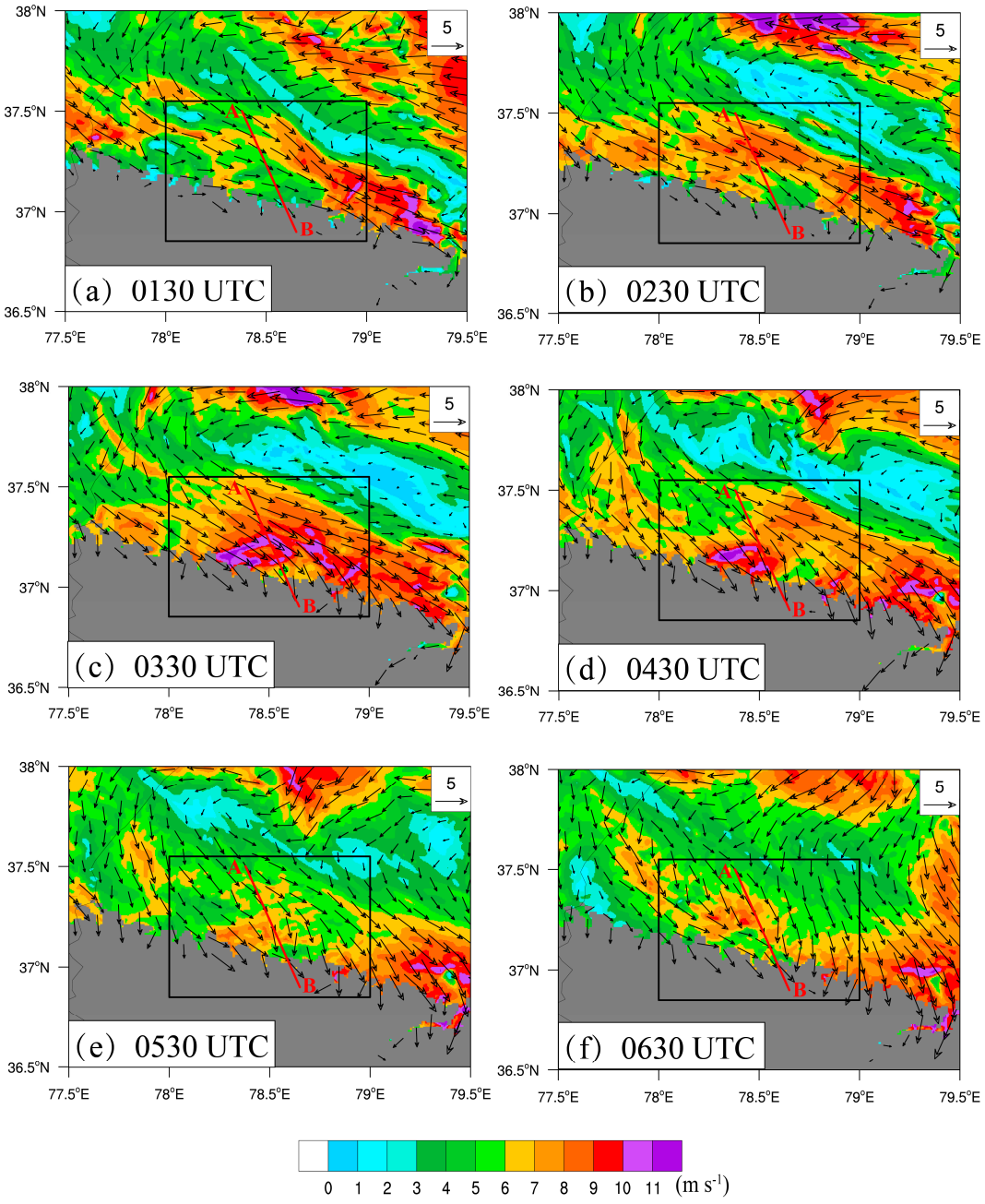

Figure S5. (a-f) the horizontal wind speed (shading, units: m s^{-1}) and the horizontal wind field (black vector arrows) at 2500 m ASL at 0130, 0230, 0330, 0430, 0530 and 0630 UTC on 15 June 2021, respectively. The gray shaded area indicates altitudes higher than 2500 m. The black rectangular box represents the specific study area.

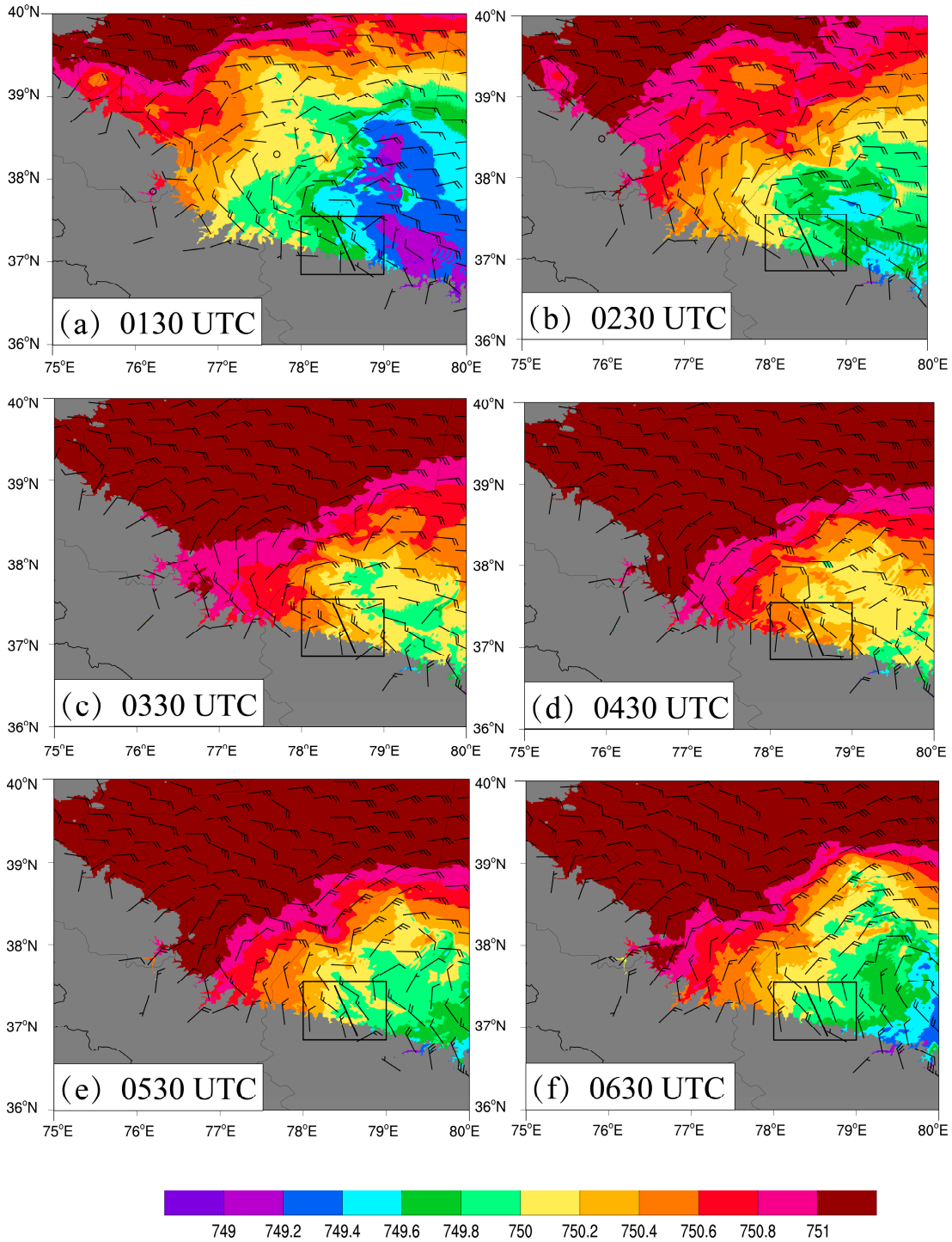

Figure S6. (a-f) the atmospheric pressure (shading, units: hPa) and wind information(wind barbs, half barbs, full barbs, and flags represent 2, 4, and 20 m s^{-1}, respectively) at 2500 m ASL at 0130, 0230, 0330, 0430, 0530 and 0630 UTC on 15 June 2021, respectively. The gray shaded area indicates altitudes higher than 2500 m. The black rectangular box represents the specific study area.

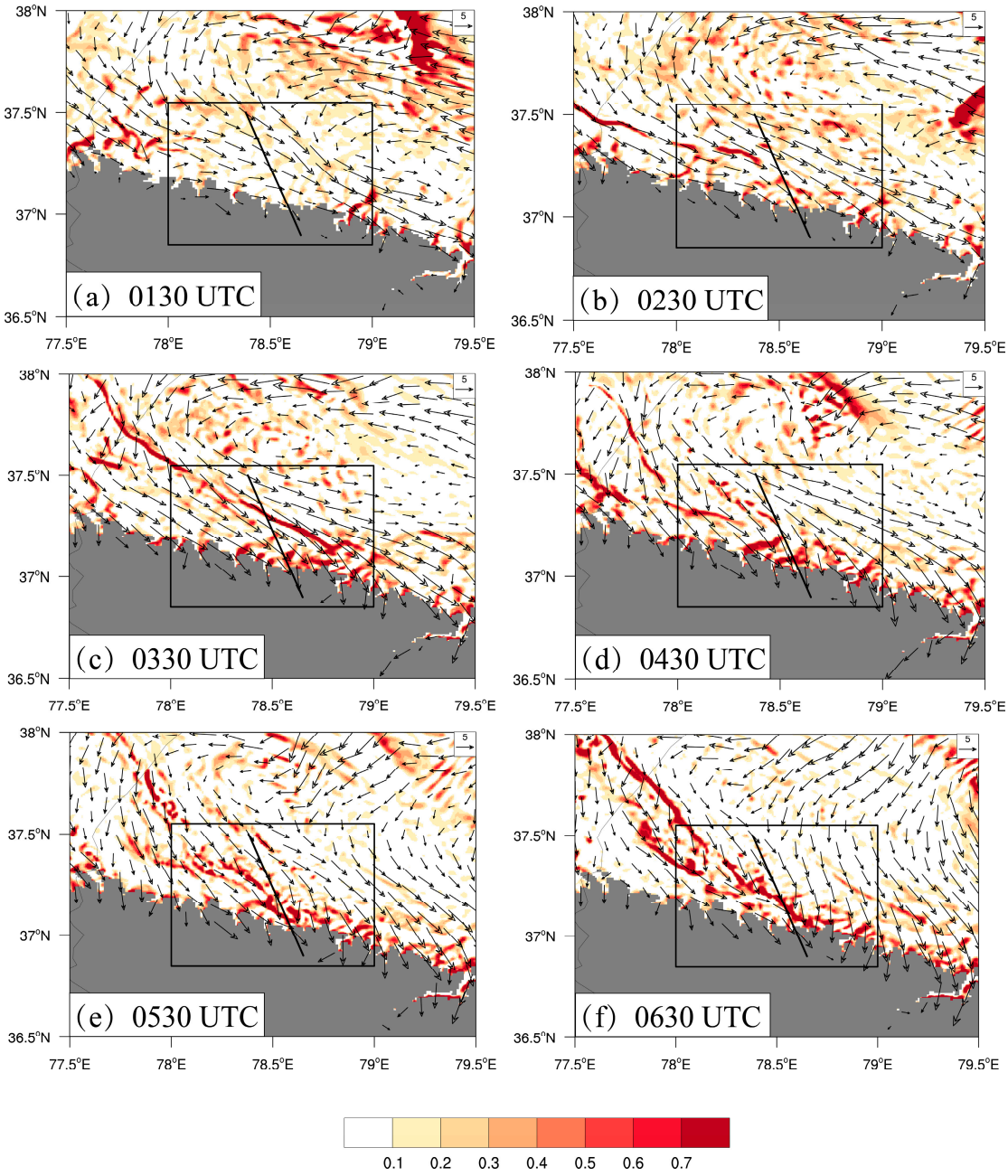

Figure S7. (a-f) the vertical speed (shading, units: m s^{-1}) and the horizontal wind field (black vector arrows) at 2500 m ASL at 0130, 0230, 0330, 0430, 0530 and 0630 UTC on 15 June 2021, respectively. The gray shaded area indicates altitudes higher than 2500 m. The black rectangular box represents the specific study area.

References:

Zhang, D.L. and Cho, H.R. The development of negative moist potential vorticity in the stratiform region of a simulated squall line. *Mon.Weather Rev*., 1992, 120, 1322–1341.

Wu Guoxiong, Cai Yaping, Tang Xiaojing. Moist potential vorticity and slantwise vorticity development. *Acta Meteorologica Sinica (in Chinese)* 1995, 53(4): 387−405.

Yao X, Gao Y, Ma J. MPV-Q∗ view of vorticity development in a saturated atmosphere[J]. *Atmospheric Research*, **2020**, 244: 105058.

Gao S T, Lei T, Zhou Y. Moist potential vorticity anomaly with heat and mass forcings in torrential rain systems. *Chinese Physics Letters*, 2002, 19(6): 878-880. doi:10.1088/0256-307X/19/6/340

Schultz, D.M.; Schumacher, P.N. The use and misuse of conditional symmetric instability. Mon. Weather Rev. 1999, 127, 2709–2732,

Ullah, K.; Gao, S. A diagnostic study of convective environment leading to heavy rainfall during the summer monsoon 2010 over Pakistan. Atmospheric Research, 2013, 120, 226-239.

Liu, J.; Liu, Z. X.; Zhang, J. R.; et al. Comparative Analysis of convection initiation Mechanism in Typical Rainstorm Events in Hami Area, Eastern Tianshan Mountains. Atmospheric Science, 2022.46(04), 965-988.

Du Y, Zhang Q, Chen Y, et al. Numerical simulations of spatial distributions and diurnal variations of low-level jets in China during early summer[J]. Journal of climate, 2014, 27(15): 5747-5767.